



Low-frequency spin dynamics of the quasi-two-dimensional $S = \frac{1}{2}$ antiferromagnet $\text{BaCdVO}(\text{PO}_4)_2$

T. A. Soldatov  and A. I. Smirnov *P. L. Kapitza Institute for Physical Problems, RAS, 119334 Moscow, Russia*

(Received 14 December 2022; revised 3 May 2023; accepted 5 May 2023; published 16 May 2023)

A quasi-two-dimensional quantum magnet with competing ferro- and antiferromagnetic exchange interactions, $\text{BaCdVO}(\text{PO}_4)_2$, is studied using the magnetic resonance technique in a wide frequency range. The magnetic resonance spectra of the ordered phase confirm the collinear antiferromagnetic spin structure oriented along the a axis. The frequency-field diagram of antiferromagnetic resonance demonstrates two low-frequency excitation branches with different energy gaps, indicating a biaxial nature of anisotropy. We observe a critical softening of the longitudinal resonance mode in a field of 3.8 T, which is the lower boundary of a previously proposed presaturation phase positioned below the saturation field of 6.5 T. An interpretation of the presaturation phase as a state with variable magnetization of spin-vacancy defects is proposed. It may be considered an alternative to the spin-nematic phase initially supposed.

DOI: [10.1103/PhysRevB.107.174423](https://doi.org/10.1103/PhysRevB.107.174423)

I. INTRODUCTION

Frustrated spin systems attract interest because their low-temperature properties are strongly influenced by quantum fluctuations. The special type of frustration provided by competing ferro- and antiferromagnetic interactions may lead to the formation of the novel nematic spin ordering near the saturation field, as found in numerical and analytical calculations [1–6]. This nematic ordering spontaneously breaks spin-rotational symmetry but conserves time-reversal symmetry [7]. The nematic state has no long-range order of spin components; there is long-range order of spin-spin correlations. The competing ferro- and antiferromagnetic exchanges are known to be present in, e.g., zigzag spin chains like that of LiCuVO_4 [8] and square lattices with ferromagnetic nearest-neighbor exchange and antiferromagnetic diagonal exchange as in crystals of vanadium phosphates [9].

Recent papers [10–13] considered the quasi-two-dimensional (quasi-2D) $S = \frac{1}{2}$ vanadium-phosphate magnet with competing interactions $\text{BaCdVO}(\text{PO}_4)_2$ as a candidate for the realization of the nematic phase before saturation. Indeed, experiments detected an additional phase transition before saturation. This novel presaturation phase was presumed to be a quantum spin nematic state as “it is fully consistent with the expectations for a quantum bond-nematic state” [11].

A recent theoretical work [14], however, predicted that the nematic phase should occupy only a very narrow field range near the saturation field, contrary to the observed presaturation phase extending to an interval of about 30% of the saturation field.

In the present work we perform an electron spin resonance (ESR) investigation of $\text{BaCdVO}(\text{PO}_4)_2$ in both antiferromagnetically ordered and high-field phases, searching for changes in excitation spectra at these novel phase transitions and looking for spin-resonance modes of the nematic phase. However, we did not find new magnetic resonance signals in the field range between the collapse of the antiferromagnetic order and

full saturation. On the basis of these observations we propose an alternative scenario for the presaturation phase.

II. CRYSTAL STRUCTURE AND MAGNETIC PROPERTIES OF $\text{BaCdVO}(\text{PO}_4)_2$

Crystals of $\text{BaCdVO}(\text{PO}_4)_2$ have a layered structure with V^{4+} magnetic ions ($S = \frac{1}{2}$). The lattice is very close to a quadratic one but has a weak orthorhombic distortion. At room temperature $\text{BaCdVO}(\text{PO}_4)_2$ belongs to the orthorhombic P_{bca} space group with lattice parameters $a = 8.84 \text{ \AA}$, $b = 8.92 \text{ \AA}$, and $c = 19.37 \text{ \AA}$ and V^{4+} layers parallel to the (ab) planes [10]. There are eight magnetic ions in a crystallographic unit cell, four ions in each layer within a cell. Below the structural transition at $T = 250 \text{ K}$ the crystal symmetry is lowered to the orthorhombic P_{ca2_1} space group [11]. Lattice parameters of the low-temperature phase are $a = 8.8621 \text{ \AA}$, $b = 8.8911 \text{ \AA}$, and $c = 18.8581 \text{ \AA}$. In contrast to the high-temperature phase with equivalent V^{4+} ions there are two inequivalent V^{4+} positions in the low-temperature phase [11]. This results in the alternation of the exchange interaction network, which enables an exotic four-sublattice up-up-down-down (UDD) antiferromagnetic structure of a collinear type [11]. This structure was, indeed, observed in Ref. [12]. The on-site ordered moment is directed along the a axis and strongly reduced to $0.34\mu_B$ [12]. The magnetic unit cell is doubled along the b direction with respect to the crystallographic cell.

A simple two-exchange ($J_1 - J_2$) model was suggested to interpret experimental data at the first stage [15,16]. Here J_1 is the nearest-neighbor ferromagnetic exchange along the side of the square, and J_2 is the next-nearest-neighbor antiferromagnetic coupling along the diagonal of the square [see Fig. 1(a)]. Exchange constants $J_1 = -3.60 \text{ K}$ and $J_2 = 3.25 \text{ K}$ were estimated with the use of powder samples from the analysis of the susceptibility data [15]. This model is a ground for the expectation of a nematic phase just below the saturation

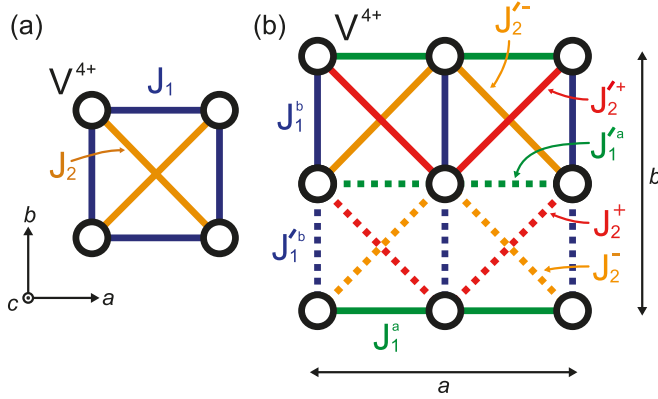


FIG. 1. Schematic representation of exchange interactions in V^{4+} layers of $BaCdVO(PO_4)_2$. (a) Simple $J_1 - J_2$ square-lattice model. (b) Model with alternation of exchange couplings along the crystallographic b axis.

[2,6], but it does not directly correspond to the observed four-sublattice Uudd structure.

A more realistic model of the exchange network was used to interpret inelastic neutron scattering data [11,13]. This model includes eight different exchange paths and is compatible with both the real crystal symmetry and four-sublattice ordering. The spin-wave spectra in the fully saturated phase were well reproduced using the following exchange parameters: $J_1^a = -1.6$ K, $J_1^b = -7.1$ K, $J_2^+ = 4.5$ K, $J_2^- = 4.2$ K, $J_2^{'+} = 0.5$ K, and $J_2^{'-} = 2.1$ K [11,13].

The long-range magnetic order with a doubled period of a unit cell [propagation vector $(0, 1/2, 0)$] occurs at the Néel temperature $T_N = 1.05$ K [10,15]. The neutron scattering measurements [11,12] show that this magnetic order disappears in a magnetic field $H_{c1} = 4$ T (at the temperature of 0.1 K). Magnetic structures with different propagation vectors were not found in higher fields. At the same time the magnetization saturation occurs only in a field $H_{c2} = 6.5$ T, although the total change in the magnetic moment between H_{c1} and H_{c2} is only 2.5% [11]. Thus, an unusual feature of $BaCdVO(PO_4)_2$ is the disappearance of the antiferromagnetic order before full saturation. Specific heat and magnetocaloric measurements also demonstrate phase transitions for $\mathbf{H} \parallel a, c$ at H_{c1} , then at an intermediate field H^* , and, finally, at H_{c2} [11].

III. EXPERIMENTAL DETAILS

Single-crystalline samples of $BaCdVO(PO_4)_2$ investigated in our experiments are from the same batch as that used in previous thermodynamic and neutron scattering measurements [10,11]. They have the form of rectangular plates with the c axis normal to the plane.

Resonance measurements were carried out with the use of a homemade transmission-type ESR spectrometer equipped with a superconducting 12 T magnet and ^3He cryostat providing temperatures down to 0.45 K. Microwave units with cylindrical, rectangular, and cut-ring copper resonators were used to record the resonance absorption of microwaves. To cover a wide frequency range of 2–150 GHz we used Gunn

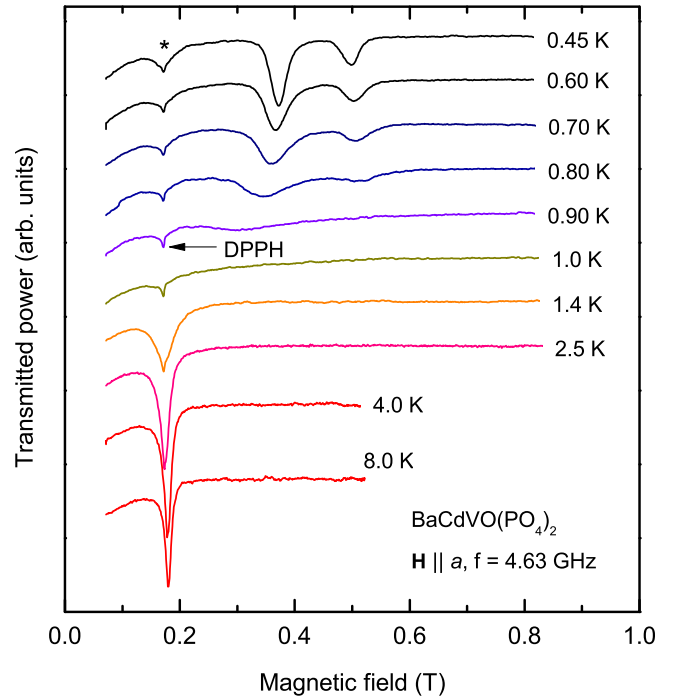


FIG. 2. Temperature evolution of the ESR line for $\mathbf{H} \parallel a$ at $f = 4.63$ GHz. The star marks the paramagnetic resonance absorption. The DPPH resonance peak is a $g = 2.00$ marker. The temperature-independent decrease of the transmitted signal below 0.12 T is an apparatus effect.

diodes, back-wave oscillators, and klystrons as microwave sources. Crystal samples were mounted inside resonators at the maximum of the microwave magnetic field, polarized perpendicular to the external field. If necessary, we used parallel polarization for records of longitudinal modes. A small amount of 2,2-diphenyl-1-picrylhydrazyl (DPPH) was placed near the sample as a standard $g = 2.00$ marker. For experiments at different frequencies we used samples with masses from 0.5 to 12 mg. The size of a sample was chosen to be compatible with a resonator volume and Q factor and to be small enough to avoid parasitic electrodynamic resonances in the sample. There was no difference in resonance fields for different samples used.

Records of ESR absorption lines were made as field dependences of microwave power passed through the resonator during a sweep of the external magnetic field. Modulation of the microwave power and lock-in measurement of the transmitted signal were used for noise reduction.

IV. EXPERIMENTAL RESULTS

The temperature evolution of ESR lines for three principal field orientations, $\mathbf{H} \parallel a, b, c$, is presented in Figs. 2–4. At temperatures above 2 K we observe a single ESR absorption line. In the whole frequency range its resonance field corresponds to a temperature-independent g tensor with principal values $g_a = g_b = 1.97 \pm 0.01$ and $g_c = 1.91 \pm 0.01$, which are in agreement with susceptibility data in Ref. [10].

The absorption spectrum significantly changes after crossing the transition temperature $T_N = 1.05$ K. ESR lines

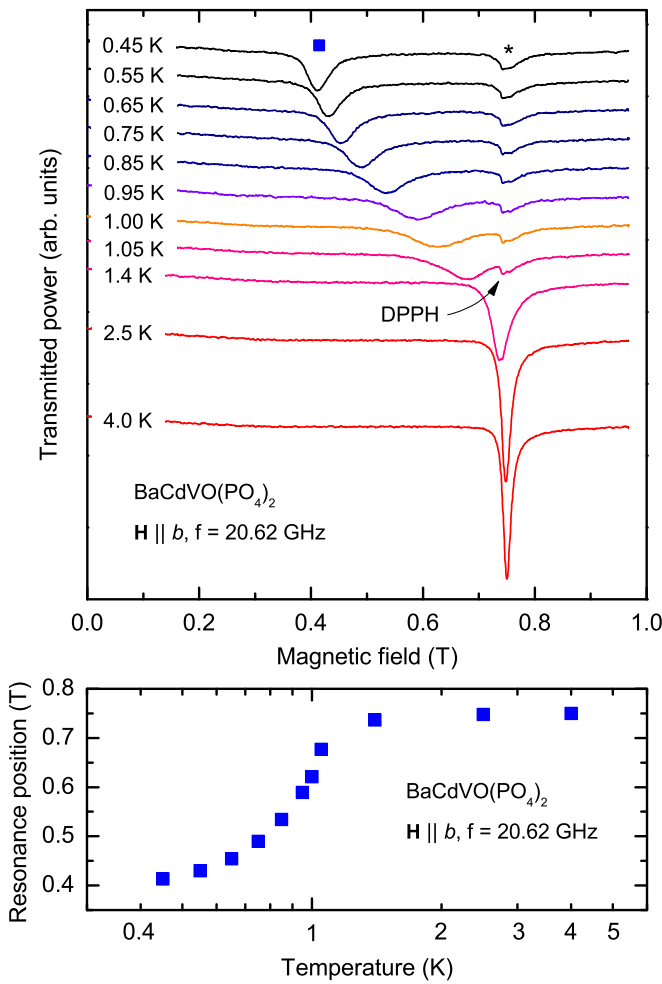


FIG. 3. Top: temperature evolution of the ESR line for $\mathbf{H} \parallel b$ at $f = 20.62$ GHz; the star marks the paramagnetic resonance absorption, and the solid square is at the low-temperature antiferromagnetic resonance field. The DPPH resonance field is a $g = 2.00$ marker. Bottom: temperature dependence of the ESR field.

measured at $\mathbf{H} \parallel b, c$ demonstrate broadening and shifting to lower fields upon cooling (see Figs. 3 and 4). In contrast to $\mathbf{H} \parallel b, c$, for $\mathbf{H} \parallel a$, two new ESR lines appear below T_N , and the low-frequency resonance fields are shifted towards higher fields (see Fig. 2). The zero-temperature limit for resonance positions is almost reached at around 0.5 K since the evolution is already slow at this temperature. The corresponding temperature dependence of the ESR field at $\mathbf{H} \parallel b$ is illustrated in the bottom panel of Fig. 3.

Weak absorption, marked by stars in Figs. 2–10, continues to be observable below T_N at the paramagnetic resonance field for all field orientations. The resonance field of this absorption and its integral intensity were determined by fitting the absorption curves with Lorentzians. The intensity of this mode grows with cooling following Curie's law $1/T$, and its position is temperature independent and corresponds to a paramagnetic resonance field $H_{PM} = 2\pi\hbar f / (g\mu_B)$, where f is the microwave frequency. Therefore, this resonance is probably due to a small number of paramagnetic impurities or defects in the crystal. The concentration of these defects may

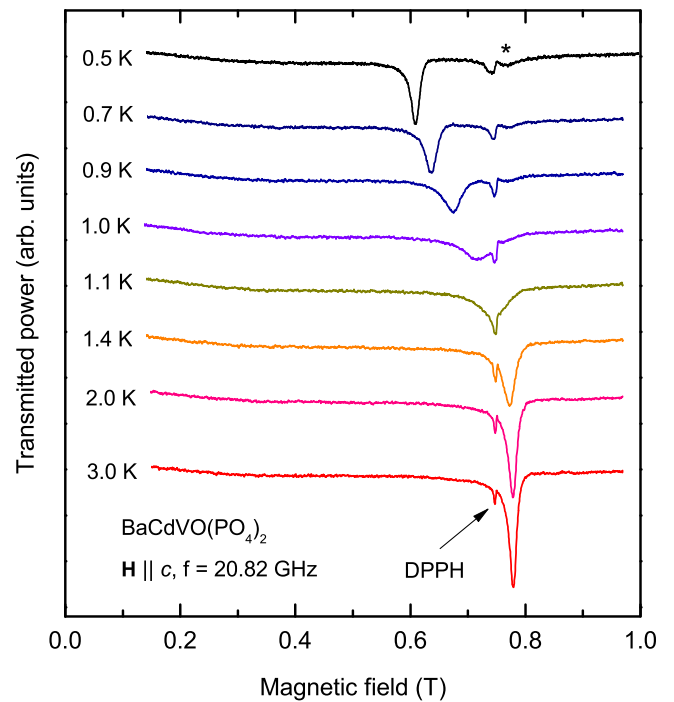


FIG. 4. Temperature evolution of the ESR line for $\mathbf{H} \parallel c$ at $f = 20.82$ GHz. The star marks the paramagnetic resonance absorption. The DPPH resonance field is a $g = 2.00$ marker.

be estimated from the integral intensity of the low-temperature paramagnetic resonance lines presented in Fig. 4 to be about 0.03 of the total number of V^{4+} ions. The ESR signal of the sample in the paramagnetic phase at a temperature of 8 K was used as a reference for a known number of magnetic ions obeying Curie's law. The Curie-Weiss temperature is known to be small in absolute value, $\Theta_{CW} = -0.9$ K [10].

Frequency-field diagrams together with examples of ESR lines for different frequencies taken at 0.5 K for $\mathbf{H} \parallel a, b, c$ in the low-field range are shown in Figs. 5–7. Resonance fields were determined as fields of maximum microwave absorption; they are marked on the panels with ESR lines in Figs. 5–9 by symbols. The error in the resonance field does not exceed the size of a symbol. The same symbols are used in the frequency-field diagrams in Figs. 5–9; their size exceeds the error in resonance field.

All frequency-field diagrams show two modes of resonance absorption with different zero-field energy gaps, Δ_1 and Δ_2 ($\Delta_1 < \Delta_2$). With increasing magnetic field applied parallel to the a axis we observe a branch with the zero-field gap Δ_2 initially rising and then demonstrating a vertical frequency drop at $H_{sf} = 0.46$ T (spin-flop field according to Ref. [10]). A branch with the zero-field gap Δ_1 has a gradually falling frequency which may be extrapolated to zero at H_{sf} . In the field above H_{sf} we observe, again, the ascending branch starting from zero frequency at H_{sf} , as shown by the frequency-field dependence in Fig. 5.

For $\mathbf{H} \parallel c$ the Δ_1 mode has a monotonically increasing field dependence of the resonance frequency, while at $\mathbf{H} \parallel b$ the Δ_2 mode increases. At the same time, for $\mathbf{H} \parallel a$ and $\mathbf{H} \parallel b$ we observe that the Δ_1 mode, which has a constant frequency in low field, begins to fall above 1.5 T and demonstrates

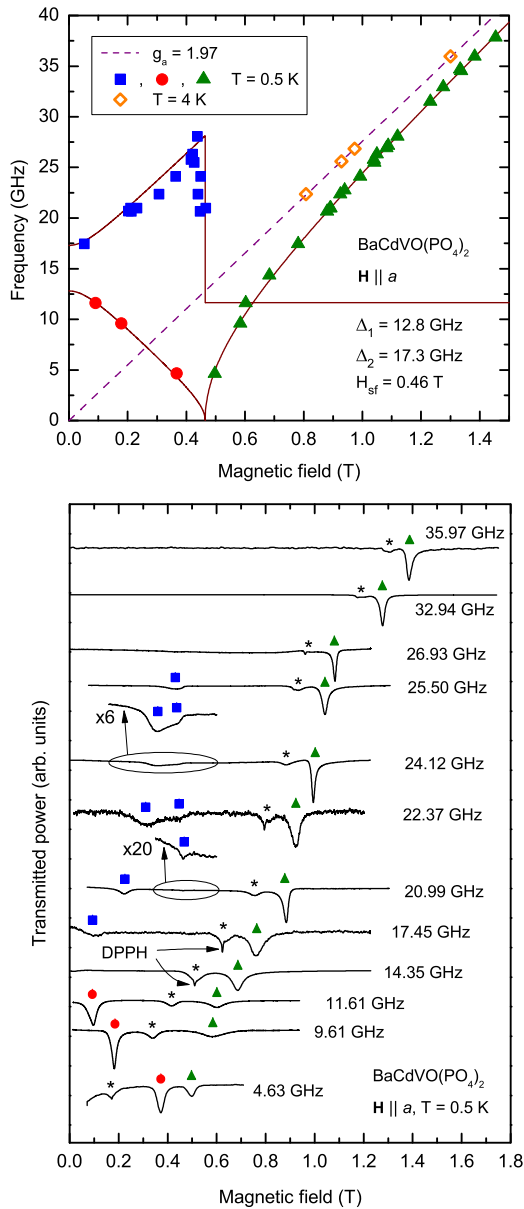


FIG. 5. Top: the frequency-field diagram for $\mathbf{H} \parallel a$. Solid symbols correspond to $T = 0.5$ K; open symbols correspond to $T = 4$ K. The dashed line corresponds to a paramagnetic resonance with $g_a = 1.97$. Solid lines are theoretical curves (1) and (2). Bottom: examples of ESR lines at $\mathbf{H} \parallel a$, $T = 0.5$ K. Stars label modes of parasitic paramagnetic absorption. Other solid symbols indicate the positions of resonance modes marked in the frequency-field diagram.

complete softening at 3.8 T (see Figs. 8 and 9). This field corresponds well to the value of H_{c1} at $T = 0.5$ K. It is worth noting that this softening was studied in a special experiment with polarization of the microwave magnetic field along the external field. This was necessary because the experimental polarization dependence of the absorption for this mode shows the oscillating component of the magnetic moment along the external field, while at a conventional ESR precessing magnetization is perpendicular to the external field [17].

The top panel of Fig. 10 demonstrates the frequency-field diagram obtained at 0.5 K for $\mathbf{H} \parallel c$ in the field range includ-

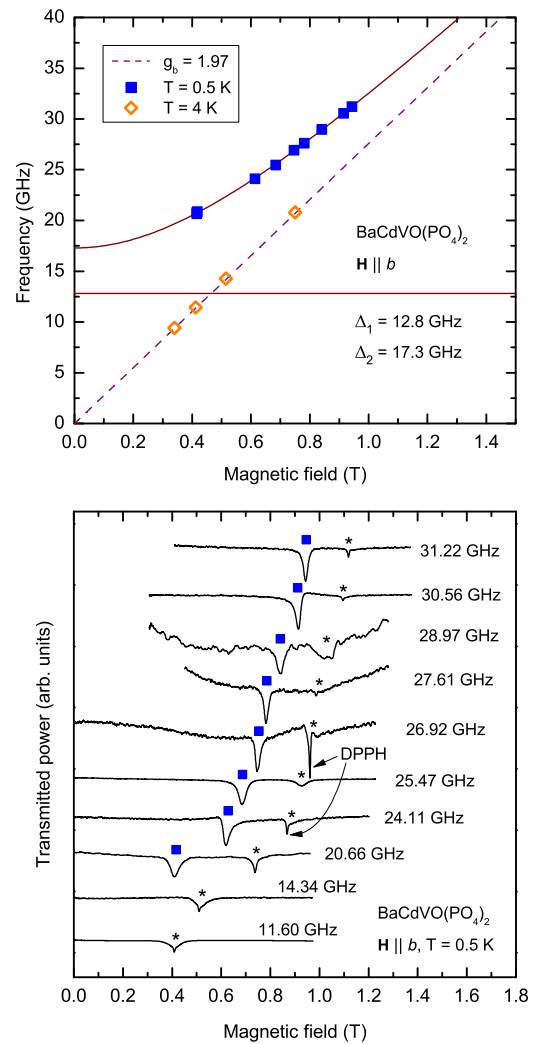


FIG. 6. Top: the frequency-field diagram for $\mathbf{H} \parallel b$. Solid symbols correspond to $T = 0.5$ K; open symbols correspond to $T = 4$ K. The dashed line corresponds to a paramagnetic resonance with $g_b = 1.97$. Solid lines are theoretical curves (3). Bottom: examples of ESR lines measured for $\mathbf{H} \parallel b$ at $T = 0.5$ K. Stars label parasitic paramagnetic modes. Other solid symbols indicate the positions of resonance modes marked in the frequency-field diagram.

ing the presaturation phase $H_{c1} < H < H_{c2}$ for the upper part of the frequency range. The bottom panel presents examples of absorption curves. At fields $H_{c1} < H < H_{c2}$ only a single resonance mode with Larmor frequency was observed.

V. DISCUSSION

The low-frequency dynamics of a collinear multisublattice antiferromagnet may be described in a general form by the macroscopic theory in Ref. [18]. It considers, in particular, an arbitrary collinear antiferromagnetic structure with any number of sublattices and is suitable for the four-sublattice case of $\text{BaCdVO}(\text{PO}_4)_2$. This theory is, however, restricted to low-frequency dynamics with frequencies far below the exchange range and to fields far below saturation, where the spin structure is not strongly distorted by the magnetic field. This approach results in the same spectra of spin oscillations that

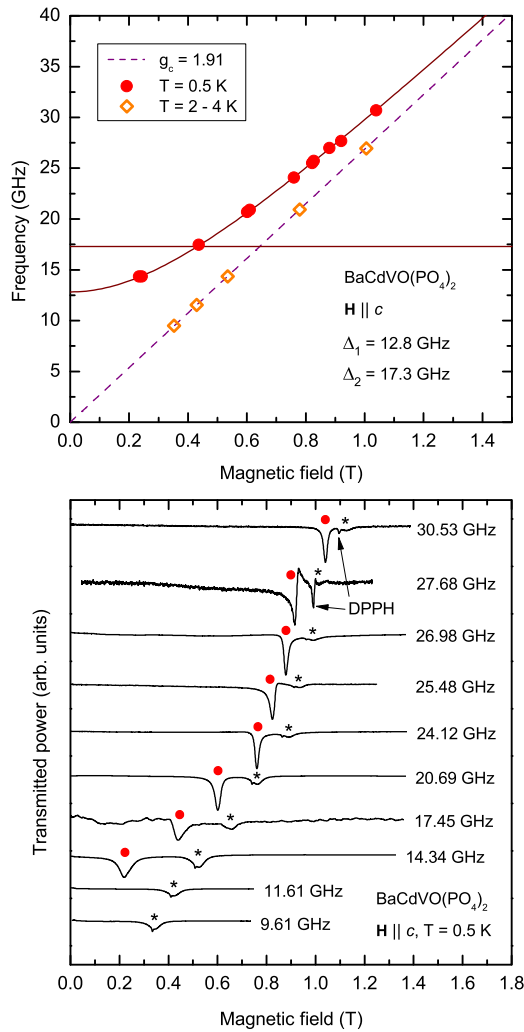


FIG. 7. Top: the frequency-field diagram for $\mathbf{H} \parallel c$. Solid symbols correspond to $T = 0.5$ K; open symbols correspond to $T = 2 - 4$ K. The dashed line corresponds to a paramagnetic resonance with $g_c = 1.91$. Solid lines are theoretical curves (4). Bottom: examples of ESR lines measured for $\mathbf{H} \parallel c$ at $T = 0.5$ K. Stars label parasitic paramagnetic modes. Other solid symbols indicate the positions of resonance modes marked in the frequency-field diagram.

were obtained using the mean-field theory for a well-known particular case of a two-sublattice collinear antiferromagnet (see, e.g., Ref. [19]). However, one should note that the high-frequency modes of the exchange-frequency range are not suitable for calculating by macroscopic theory [18]. Thus, macroscopic theory results in only two of four expected resonance modes of the UDD structure.

For a collinear antiferromagnet with a biaxial type of anisotropy the macroscopic approach was developed in, e.g., [20]. For magnetic field applied along the a axis, below the spin-flop transition field H_{sf} , the macroscopic theory gives

$$f_{1,2}^2 = (\gamma_a H)^2 + \frac{\Delta_1^2 + \Delta_2^2}{2} \mp \sqrt{2(\Delta_1^2 + \Delta_2^2)(\gamma_a H)^2 + \frac{(\Delta_2^2 - \Delta_1^2)^2}{4}}, \quad (1)$$

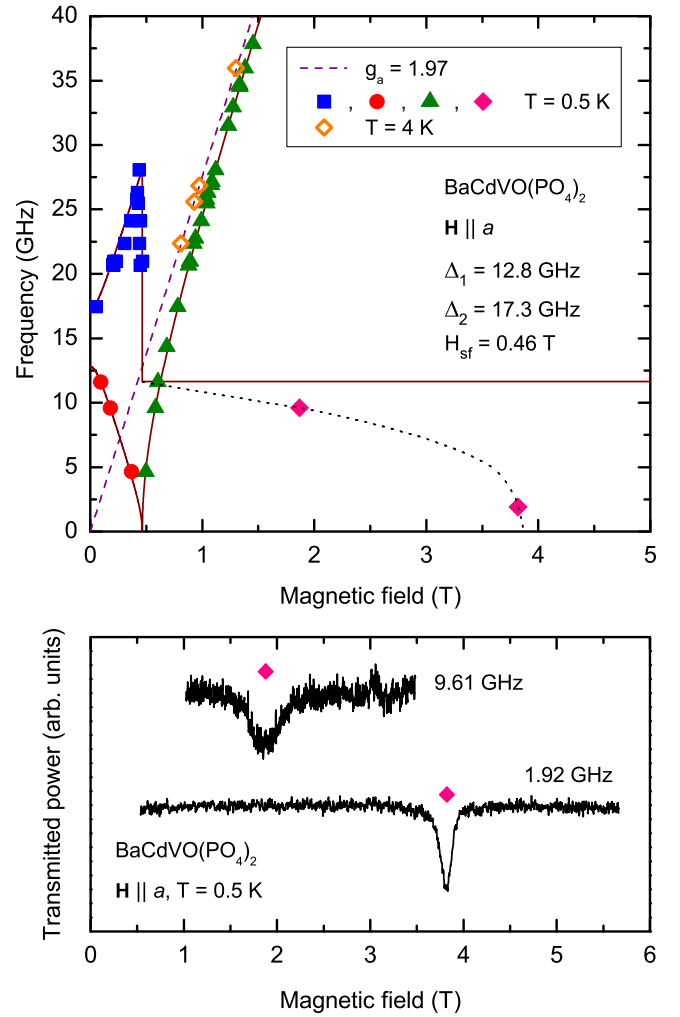


FIG. 8. Top: the frequency-field diagram for $\mathbf{H} \parallel a$ in a wide magnetic field range. Solid symbols correspond to $T = 0.5$ K; open symbols correspond to $T = 4$ K. The dashed line corresponds to a paramagnetic resonance with $g_a = 1.97$. Solid lines are theoretical curves (1) and (2). The dotted line is a guide to the eye. Bottom: ESR lines for $\mathbf{H} \parallel a$ at $T = 0.5$ K within the subgap frequency range. Solid symbols indicate positions of the soft mode marked in the frequency-field diagram.

where $\gamma_a = g_a \mu_B / 2\pi \hbar$ and $\Delta_{1,2}$ are the energy gaps expressed in terms of macroscopic anisotropy constants and macroscopic susceptibility. The spin-flop transition field is expressed as $H_{sf} = \Delta_1 / \gamma_a$.

Above the spin-flop transition field the frequencies are given by

$$f_1 = \sqrt{\Delta_2^2 - \Delta_1^2}, \quad f_2 = \sqrt{(\gamma_a H)^2 - \Delta_1^2}. \quad (2)$$

For $\mathbf{H} \parallel b$ the macroscopic theory (see, e.g., [20]) gives

$$f_1 = \Delta_1, \quad f_2 = \sqrt{(\gamma_b H)^2 + \Delta_2^2}, \quad (3)$$

whereas for $\mathbf{H} \parallel c$ —

$$f_1 = \sqrt{(\gamma_c H)^2 + \Delta_1^2}, \quad f_2 = \Delta_2, \quad (4)$$

where $\gamma_b = g_b \mu_B / 2\pi \hbar$ and $\gamma_c = g_c \mu_B / 2\pi \hbar$.

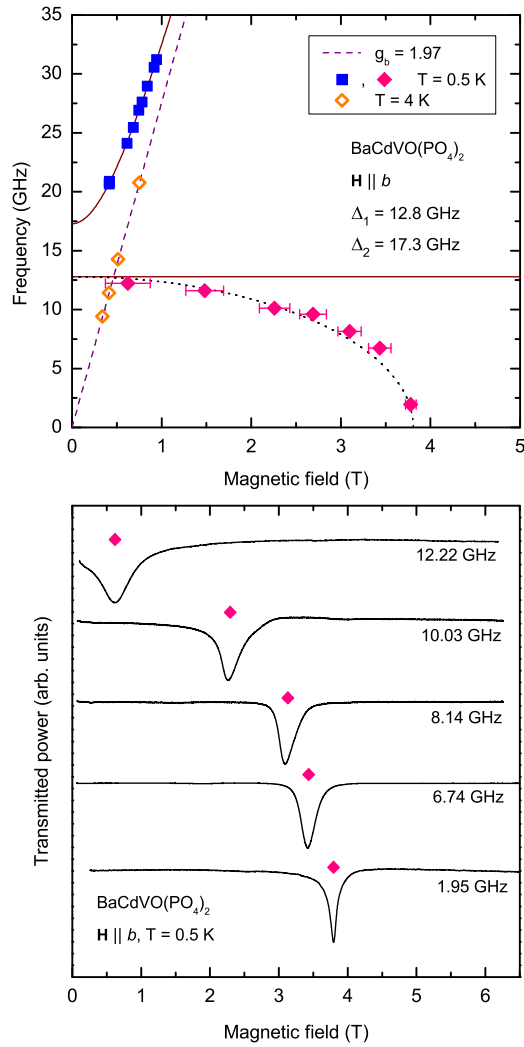


FIG. 9. Top: the frequency-field diagram for $\mathbf{H} \parallel b$ in a wide magnetic field range. Solid symbols correspond to $T = 0.5$ K; open symbols correspond to $T = 4$ K. The dashed line represents the paramagnetic resonance with $g_b = 1.97$, Solid lines are theoretical curves (3). The dotted line is plotted according to relation (5) with $\Delta_0 = 12.8$ GHz and $H_{\text{sat}} = 3.81$ T. Error bars on the lower branch correspond to the width at the half height for resonance lines presented in the bottom panel. Bottom: ESR lines measured for $\mathbf{H} \parallel b$ at $T = 0.5$ K within the subgap frequency range. Solid symbols indicate positions of the soft mode marked in the frequency-field diagram.

Here we empirically use the magnetic field terms with the anisotropic factors γ_α instead of the isotropic γ in the initial theories [18,19]. This empiric change in parameters results in a 1.5% correction of the resonance frequency at $\mathbf{H} \parallel b, c$ and a 4% correction at $\mathbf{H} \parallel a$.

The problem of the g factor anisotropy for antiferromagnetic resonance frequencies was recently studied using the spin-wave formalism [21]. In a related case, this consideration justifies the use of the values of g_a, g_b , and g_c instead of the isotropic value $g = 2$ for the symmetric orientations of the external field.

By fitting the experimental frequency-field dependences for $\mathbf{H} \parallel b$ and $\mathbf{H} \parallel c$ with relations (3) and (4) in the field

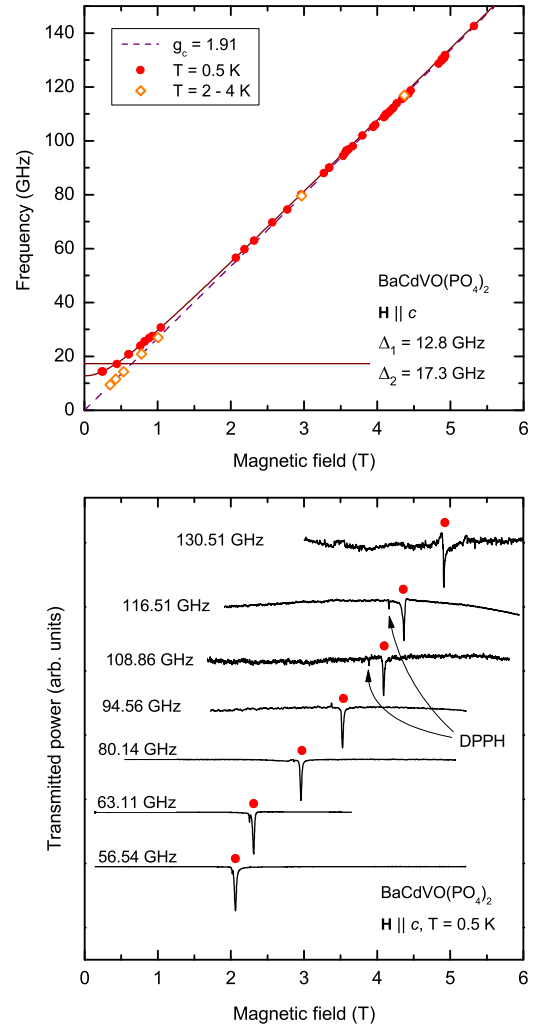


FIG. 10. Top: the frequency-field diagram for $\mathbf{H} \parallel c$ within the wide frequency and magnetic field range. Solid symbols correspond to $T = 0.5$ K; open symbols correspond to $T = 2-4$ K. The dashed line represents the paramagnetic resonance with $g_c = 1.91$. Solid lines are theoretical curves (4). Bottom: examples of ESR lines measured for $\mathbf{H} \parallel c$ at $T = 0.5$ K. Solid symbols indicate the positions of resonance modes marked in the frequency-field diagram.

range below 1.5 T we obtain the values of zero-field gaps $\Delta_1 = 12.8 \pm 0.5$ GHz and $\Delta_2 = 17.3 \pm 0.5$ GHz. Results of the fitting are shown in Figs. 6 and 7. The frequency-field dependence calculated for $\mathbf{H} \parallel a$ according to Eqs. (1) and (2) is plotted in the top panel of Fig. 5. The g_α values were measured by paramagnetic resonance measurements at high temperature. Both rising and falling branches as well as a change in the spectrum at the spin-flop transition correspond well to the theoretical predictions.

Thus, the low-frequency, low-field part of the spectrum of magnetic resonance is fully consistent with the low-temperature dynamics of a collinear antiferromagnet with biaxial anisotropy [19,20]. It allows us to identify the a axis as an easy axis because a characteristic vertical drop in the frequency indicates a spin-flop transition. The b axis is identified as a hard axis of the spin ordering because here we observe

an ascending branch starting at the larger zero-field gap Δ_2 , in accordance with theory.

At a further increase of field the agreement with macroscopic theory naturally gets worse (see Figs. 8 and 9) because the exchange spin structure becomes strongly distorted by the magnetic field. The frequency of a resonance mode which is approximately constant below a field of 1 T becomes smaller and finally drops to zero at a magnetic field of 3.8 T. In a conventional two-sublattice collinear antiferromagnet this mode approaches zero frequency exactly at the field of parallel orientation of antiferromagnetic sublattices, i.e., at the disappearance of the antiferromagnetic order parameter for a two-sublattice model [22]. The result of this calculation may be parametrized in the form given in Ref. [20] (see also Ref. [21]):

$$f = \Delta_0 \sqrt{1 - \left(\frac{H}{H_{\text{sat}}}\right)^2}. \quad (5)$$

This frequency-field dependence is presented in the top panel of Fig. 9 by the dotted curve without fitting parameters. The value $\Delta_0 = 12.8$ GHz is taken from the fit of the low-field data presented in Figs. 6 and 7. Here we take for H_{sat} the value of $H_{c1} = 3.81$ T measured for $T = 0.5$ K in Ref. [11].

Our measurements show that for $\mathbf{H} \parallel b$ and $\mathbf{H} \parallel a$ the antiferromagnetic mode with the zero-field gap Δ_1 reaches zero frequency at H_{c1} . In addition, in the field interval between H_{c1} and H_{c2} there are no resonances between the lowest frequency of our measurements (1.95 GHz) and the paramagnetic resonance frequency $f_{\text{PM}} = g_b \mu_B H / 2\pi \hbar$.

To interpret these results we should compare the scenarios for an immediate transition from an antiferromagnetic phase to the saturated phase and a transition to a presaturation nematic phase. At the immediate transition from the antiferromagnetic phase to saturated phase, the frequency of the lowest mode reaches zero, and the mode disappears. This scenario is confirmed by the mentioned mean-field calculation for a two-sublattice collinear antiferromagnet [22], as well as by the spin-wave calculation and experiment in Ref. [21]. Most likely, the four-sublattice collinear system of $\text{BaCdVO}(\text{PO}_4)_2$ will also follow this way, taking into account that the low-field evolution coincides perfectly with two-sublattice model. This scenario, in which the saturation field is $H_{c1} = 3.8$ T, is illustrated in Fig. 11 by solid line 1. If the saturation field is $H_{c2} = 6.5$ T, this kind of evolution should follow line 4. In principle, there may be a nonzero frequency at the saturation field (not presented in Fig. 11). Anyway, this mode should disappear above the saturation field because a quasi-Goldstone mode, occurring at spontaneously broken symmetry, disappears when high symmetry is restored. The last conclusion is illustrated, e.g., by a spin-wave calculation of the resonance frequencies of a saturated system with several different antiferromagnetic exchange bonds and four magnetic ions in a unit cell of Cs_2CuCl_4 [23]: there are only a Larmor mode and a high-frequency mode of the exchange frequency.

The theory of a spin-nematic state [7] predicts that the macroscopic properties of the spin nematic are the same as those of a conventional antiferromagnet. The macroscopic description of the low-frequency long-wave spin dynamics of the spin nematic coincides with that of a conventional

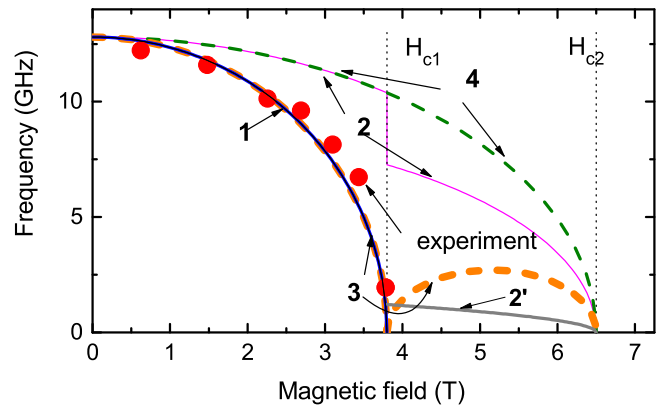


FIG. 11. Possible scenarios for the softening of the spin-flip mode at $\mathbf{H} \parallel b$. All curves represent qualitative behavior of the resonance mode in the frequency-field diagram. Curve 1 is plotted under the assumption of $H_{\text{sat}} = H_{c1}$, without the formation of a nematic phase. Curve 2 is plotted under the assumption of the formation of a spin-nematic phase between H_{c1} and H_{c2} with $H_{\text{sat}} = H_{c2}$; the nematic correlations are supposed to be conserved in the antiferromagnetic phase. Curve 3 illustrates the transition to a nematic phase with a correlator which is absent in the antiferromagnetic phase. Curve 4 is plotted under the assumption of antiferromagnetic ordering of spins until $H_{\text{sat}} = H_{c2}$. The frequency of the spin-flip mode detected experimentally at $\mathbf{H} \parallel b$ and $T = 0.5$ K is marked by solid circles. Curve 2' corresponds to a nematic phase with a magnetic resonance frequency below the experimental frequency range.

antiferromagnet with the same type of anisotropy. As a result, the magnetic resonance spectra of a spin nematic should be similar to that of an antiferromagnet, differing only by the values of the numerical parameters, i.e., of the zero-field gaps. This general conclusion in Ref. [7] is confirmed by immediate calculations of excitation frequencies for a nematic state in a $J_1 - J_2$ model [24] and for the extended model shown in Fig. 1(b) [25]. Parameters were adopted for $\text{BaCdVO}(\text{PO}_4)_2$. These calculations result in two branches of spin excitations. In an isotropic exchange approximation the first branch has a Larmor frequency at $q = 0$, while the second longitudinal mode is a Goldstone-type oscillation that is gapless at $q = 0$ and has a linear dispersion. Naturally, it should acquire a gap under the action of anisotropy. Thus, the nematic spectrum was shown to be analogous to the spectrum of an antiferromagnet on the same lattice. One should note that the nematic order parameter $Q_{ij}^{\alpha\beta}$ should be nonzero also in the antiferromagnetic phase. For example, a simple nematic correlator [7]

$$Q_{ij}^{\alpha\beta} = \langle S_i^\alpha S_j^\beta \rangle - \frac{1}{3} \delta_{\alpha\beta} \langle \mathbf{S}_i \mathbf{S}_j \rangle, \quad (6)$$

with i and j indexing lattice sites and α and β being coordinate axes, exists for a two-sublattice antiferromagnet.

Let us discuss the anticipated behavior of the resonance frequency of the lowest mode at the proposed transition from an antiferromagnetic phase to a nematic phase. The identity of the macroscopic description of magnetic resonance in nematic and antiferromagnet states implies that a quasi-Goldstone mode should exist in both phases. That is why, if a nematic exists, we should see either conservation of nonzero frequency at the crossing of the critical field H_{c1} (line 2 in Fig. 11) or the vanishing and restoration of the frequency (line 3).

Nevertheless, experimentally, we observe the above scenario presented by line 1. This means that we see no traces of a nematic phase between H_{c1} and H_{c2} .

Our observations correspond to a conventional immediate transition from an antiferromagnetic phase to a saturated phase in a field H_{c1} . The nematic phase is consistent with our observations only if the resonance frequency of its quasi-Goldstone mode is lower than the limit of our experimental range, 1.92 GHz, as presented by line 2' in Fig. 11.

A possible reason for the absence of the nematic phase may be, e.g., anisotropy. Anisotropy may reduce fluctuations and thus make a long-range antiferromagnetic order preferable to a nematic one. The anisotropy was omitted in the theoretical analysis of a nematic phase [2,14,24,25]. The observation of zero-field gaps in the antiferromagnetic resonance spectrum with significant values ($\Delta_1 = 0.61$ K, $\Delta_2 = 0.82$ K) indicates essential anisotropy. A crude estimation of the parameter D of the anisotropy energy may be obtained via the mean-field relation

$$\Delta \simeq \sqrt{DJ}\langle S \rangle, \quad (7)$$

where J is the effective exchange interaction (we take $J = 5$ K as a value for antiferromagnetic exchanges $J^{2\pm}$ and $J'^{2\pm}$) and $\langle S \rangle = 0.17$ according to Ref. [12]. The estimation gives $D \simeq 5$ K; this large value does not correspond to the usual condition for the validity of formula (7), $D \ll J$. Nevertheless, this definitely indicates that the anisotropy is large and may influence the ground state, preventing the formation of a nematic phase.

An alternative to the spin-nematic hypothesis for incomplete saturation between H_{c1} and H_{c2} may presumably be associated with a small number of defects, e.g., spin vacancies. The magnetic moments in the vicinity of a spin vacancy may not be saturated in high fields and may, in principle, provide the peculiarities in specific heat and magnetocaloric measurements observed in Refs. [10,11,13]. For this scenario the true saturation field of a pure sample without defects should be H_{c1} , at which softening of the Δ_1 mode is expected. This hypothesis is consistent with our observations as well as with a rather tiny value of the magnetization growth (about 2.5% [11]) in the rather wide interval between H_{c1} and H_{c2} . The problem of magnetic saturation of defects of the antiferromagnetic structure with competing exchanges was highlighted in Ref. [8]. In this work the possibility of the formation of a spin-nematic state in magnetic field near saturation was discussed for the frustrated spin-chain antiferromagnet LiCuVO_4 . The authors concluded that defects result in a higher saturation field relative to the saturation field

of a pure sample and may lead to additional features in the magnetization curve.

In summary, two scenarios are possible according to our observations. Most likely, there is a regular saturation of the antiferromagnetic spin structure in a field of 3.8 T without realization of the nematic phase. At the same time we cannot fully exclude the case of a nematic state with an unexpectedly low resonance mode in the field range between H_{c1} and H_{c2} .

It is worth noting that the present observation of the softening of the lowest antiferromagnetic resonance mode does not have exactly the same sense as the observation of the vanishing of the magnetic Bragg peak in neutron scattering [11]. The Bragg peak should vanish in the case of the transition both to a nematic phase and to a saturated phase, while the antiferromagnetic resonance frequency should vanish only at the transition to the saturated phase. Thus, the observed simultaneous softening of the antiferromagnetic resonance mode and vanishing of a neutron Bragg peak means that the field H_{c1} is most likely the field of a transition to a saturated phase.

VI. CONCLUSIONS

A detailed ESR study of the frustrated quantum magnet $\text{BaCdVO}(\text{PO}_4)_2$ was performed. We observed low-frequency spin-resonance modes with two distinct zero-field gaps. The measured spectra were quantitatively described by a model including the biaxial anisotropy. Approaching the saturation field, we uncovered the softening of one of these modes. It occurs exactly at the vanishing of antiferromagnetic order, as observed in Refs. [11,12]. The interpretation of this presaturation phase as the spin nematic one reported in Refs. [10–13] is inconsistent with the vanishing of the magnetic resonance frequency before saturation and may be argued by the alternative model including defects. The observed energy gaps $\Delta_1 = 12.8$ GHz and $\Delta_2 = 17.3$ GHz indicate a significant anisotropy energy of about 1 K per spin which should be involved in the theoretical analysis of the possible nematic phase. The presaturation nematic phase may not be excluded if it has an extremely low energy gap.

ACKNOWLEDGMENTS

We thank the Russian Science Foundation (Grant No. 22-12-00259) and the Program of Presidium of RAS for financial support and are indebted to V. N. Glazkov, V. I. Marchenko, K. Yu. Povarov, S. S. Sosin, L. E. Svistov, and M. E. Zhitomirsky for fruitful discussions and valuable comments. We are very grateful to Z. Yan, K. Yu. Povarov, and A. Zheludev for supplying us with monocrystalline samples of $\text{BaCdVO}(\text{PO}_4)_2$.

-
- [1] A. V. Chubukov, Chiral, nematic, and dimer states in quantum spin chains, *Phys. Rev. B* **44**, 4693 (1991).
 [2] N. Shannon, T. Momoi, and P. Sindzingre, Nematic Order in Square Lattice Frustrated Ferromagnets, *Phys. Rev. Lett.* **96**, 027213 (2006).
 [3] T. Hikihara, L. Kecke, T. Momoi, and A. Furusaki, Vector chiral and multipolar orders in the spin-1/2 frustrated ferromagnetic chain in magnetic field, *Phys. Rev. B* **78**, 144404 (2008).

- [4] J. Sudan, A. Lüscher, and A. M. Läuchli, Emergent multipolar spin correlations in a fluctuating spiral: The frustrated ferromagnetic spin-1/2 Heisenberg chain in a magnetic field, *Phys. Rev. B* **80**, 140402 (2009).
 [5] M. E. Zhitomirsky and H. Tsunetsugu, Magnon pairing in quantum spin nematic, *Europhys. Lett.* **92**, 37001 (2010).
 [6] H. T. Ueda, Magnetic phase diagram slightly below the saturation field in the stacked J_1 - J_2 model in the square lattice

- with the J_C interlayer coupling, *J. Phys. Soc. Jpn.* **84**, 023601 (2015).
- [7] A. F. Andreev and I. A. Grishchuk, Spin nematics, *Zh. Eksp. Teor. Fiz.* **87**, 467 (1984) [*Sov. Phys. JETP* **60**, 267 (1984)].
- [8] N. Büttgen, K. Nawa, T. Fujita, M. Hagiwara, P. Kuhns, A. Prokofiev, A. P. Reyes, L. E. Svistov, K. Yoshimura, and M. Takigawa, Search for a spin-nematic phase in the quasi-one-dimensional frustrated magnet LiCuVO_4 , *Phys. Rev. B* **90**, 134401 (2014).
- [9] A. A. Tsirlin and H. Rosner, Extension of the spin-1/2 frustrated square lattice model: The case of layered vanadium phosphates, *Phys. Rev. B* **79**, 214417 (2009).
- [10] K. Yu. Povarov, V. K. Bhartiya, Z. Yan, and A. Zheludev, Thermodynamics of a frustrated quantum magnet on a square lattice, *Phys. Rev. B* **99**, 024413 (2019).
- [11] V. K. Bhartiya, K. Yu Povarov, D. Blosser, S. Bettler, Z. Yan, S. Gvasaliya, S. Raymond, E. Ressouche, K. Beauvois, J. Xu, F. Yokaichiya, and A. Zheludev, Presaturation phase with no dipolar order in a quantum ferro-antiferromagnet, *Phys. Rev. Res.* **1**, 033078 (2019).
- [12] M. Skoulatos, F. Rucker, G. J. Nilsen, A. Bertin, E. Pomjakushina, J. Ollivier, A. Schneidewind, R. Georgii, O. Zaharko, L. Keller, Ch. Rüegg, C. Pfleiderer, B. Schmidt, N. Shannon, A. Kriele, A. Senyshyn, and A. Smerald, Putative spin-nematic phase in $\text{BaCdVO}(\text{PO}_4)_2$, *Phys. Rev. B* **100**, 014405 (2019).
- [13] V. K. Bhartiya, S. Hayashida, K. Yu. Povarov, Z. Yan, Y. Qiu, S. Raymond, and A. Zheludev, Inelastic neutron scattering determination of the spin Hamiltonian for $\text{BaCdVO}(\text{PO}_4)_2$, *Phys. Rev. B* **103**, 144402 (2021).
- [14] Sh. Jiang, J. Romhányi, S. R. White, M. E. Zhitomirsky, and A. I. Chernyshev, Where Is the Quantum Spin Nematic? *Phys. Rev. Lett.* **130**, 116701 (2023).
- [15] R. Nath, A. A. Tsirlin, H. Rosner, and C. Geibel, Magnetic properties of $\text{BaCdVO}(\text{PO}_4)_2$: A strongly frustrated spin-1/2 square lattice close to the quantum critical regime, *Phys. Rev. B* **78**, 064422 (2008).
- [16] A. A. Tsirlin, B. Schmidt, Y. Skourski, R. Nath, C. Geibel, and H. Rosner, Exploring the spin-1/2 frustrated square lattice model with high-field magnetization studies, *Phys. Rev. B* **80**, 132407 (2009).
- [17] A. Abragam and B. Bleaney, *Paramagnetic Resonance of Transition Ions* (Clarendon, Oxford, 1970).
- [18] A. F. Andreev and V. I. Marchenko, Symmetry and the macroscopic dynamics of magnetic materials, *Usp. Fiz. Nauk* **130**, 39 (1980) [*Sov. Phys. Usp.* **23**, 21 (1980)].
- [19] T. Nagamiya, K. Yosida, and R. Kubo, Antiferromagnetism, *Adv. Phys.* **4**, 1 (1955).
- [20] V. N. Glazkov, Yu. V. Krasnikova, I. K. Rodygina, J. Chovan, R. Tarasenko, and A. Orendáčová, Splitting of antiferromagnetic resonance modes in the quasi-two-dimensional collinear antiferromagnet $\text{Cu}(\text{en})(\text{H}_2\text{O})_2\text{SO}_4$, *Phys. Rev. B* **101**, 014414 (2020).
- [21] C. W. Cho, A. Pawbake, N. Aubergier, A. L. Barra, K. Mosina, Z. Sofer, M. E. Zhitomirsky, C. Faugeras, and B. A. Pio, Microscopic parameters of the van der Waals CrSBr antiferromagnet from microwave absorption experiments, *Phys. Rev. B* **107**, 094403 (2023).
- [22] A. G. Gurevich and G. A. Melkov, *Magnitnye kolebaniya i volny* (Fizmatlit, Moscow, 1994), Paragraph 3.2 [*Magnetic Oscillations and Waves* (CRC Press, Boca Raton, FL, 1996)].
- [23] S. A. Zvyagin, D. Kamenskyi, M. Ozerov, J. Wosnitza, M. Ikeda, T. Fujita, M. Hagiwara, A. I. Smirnov, T. A. Soldatov, A. Ya. Shapiro, J. Krzystek, R. Hu, H. Ryu, C. Petrovic, and M. E. Zhitomirsky, Direct Determination of Exchange Parameters in Cs_2CuBr_4 and Cs_2CuCl_4 : High-Field Electron-Spin-Resonance Studies, *Phys. Rev. Lett.* **112**, 077206 (2014).
- [24] A. Smerald, H. T. Ueda, and N. Shannon, Theory of inelastic neutron scattering in a field-induced spin-nematic state, *Phys. Rev. B* **91**, 174402 (2015).
- [25] A. Smerald, Magnon binding in $\text{BaCdVO}(\text{PO}_4)_2$, arXiv:2003.12747.